RSC Advances

PAPER

View Article Online
View Journal | View Issue

Open Access Article. Published on 02 November 2021. Downloaded on 1/10/2026 9:48:20 AM.
This article is licensed under a Creative Commons Attribution-NonCommercial 3.0 Unported Licence.

Check for updates

Cite this: *RSC Adv.*, 2021, **11**, 35326

Photocatalytic cascade reactions and dye degradation over CdS–metal–organic framework hybrids†

Shu-Rong Li, Feng-Di Ren, Lin Wang and Yu-Zhen Chen *

Received 6th August 2021
Accepted 21st October 2021

DOI: 10.1039/d1ra05957b

rsc.li/rsc-advances

Two bifunctional CdS–MOF composites have been designed and fabricated. The hybrids exhibited synergistic photocatalytic performance toward two cascade reactions under visible light integrating photooxidation activity of CdS and Lewis acids/bases of the MOF. The composite further promoted the photodegradation of dyes benefiting from effective electron transfer between the MOF and CdS.

Cascade reactions are usually required for the synthesis of pharmaceuticals, pesticides and various fine chemicals,[1] especially for heterocyclic compounds.[1b] Typically, benzylidene malononitrile, an essential intermediate for pharmaceutical production,[1f] is normally prepared through a two-step reaction involving first oxidation of benzyl alcohol and then a Knoevenagel condensation of benzaldehyde with malononitrile.[2d] Generally, the first step is mainly concentrated on the precious metal catalysts, and usually requires organic solvent, high temperatures, or high O_2 pressures, which largely limits its large-scale application.[2] The second Knoevenagel reaction is traditionally catalyzed by weak bases under homogeneous conditions, which is not favourable for recovery and recycling of catalysts.[2c] Therefore, it is of great importance to develop a low-cost, stable and environmentally-friendly multifunctional catalyst.

Solar energy, as an abundant natural resource, has attracted significant interest in photocatalytic water splitting, CO_2 or organic substrate transformations.[3,4] However, given that natural solar radiation is scattered, intermittent and constantly fluctuating, increasing the conversion rate of solar energy into chemical energy through photosensitive materials remains to be a great challenge.[5] Significantly, a typical semiconductor material, CdS, displays excellent photocatalytic performance for many chemical reactions under light irradiation, such as photooxidation due to its a narrow band gap energy (2.4 eV) and efficient visible light absorption.[6] However, the fact that a rapid recombination of photoelectrons and holes in CdS, and easy agglomeration of CdS nanoparticles (NPs) greatly impedes its practical application.[6d,7] Therefore, stable and effective supports should be required to stabilize pure CdS NPs.

Metal organic frameworks (MOFs),[8] featuring ordered porosities and large surface areas, have been widely used to stabilize various guest molecules, including metal nanoparticles, semiconductors and quantum dots.[7,8d,9] Recently, MOF-based composites have attracted intensive attention in photocatalysis field.[5a,9f,10] Unfortunately, most MOFs exhibit a wide bandgap and only absorb ultraviolet light region.[7,11] In addition, pure MOFs generally have a single active site, largely limiting catalytic reaction types.[9d] Therefore, photoactive CdS combined with the advantages of MOFs can help construct a synergistic hybrid material.[7]

Bearing above idea in mind, we have successfully fabricated a bifunctional CdS/NH_2-MIL-125 photocatalyst based on photosensitive CdS and active NH_2-MIL-125 (Scheme 1). The cooperative effect greatly improved photocatalytic performance of the composite toward the cascade reaction of selective oxidation of benzyl alcohol to benzaldehyde tandemly with a condensation of benzaldehyde with malononitrile. The superior catalytic activity mainly benefits from excellent photooxidation activity of CdS while the outer NH_2-MIL-125 plays multiple roles; it acts as a Lewis base site, accelerates the reaction by O_2 enrichment in air atmosphere, and stabilizes the CdS cores. Furthermore, effective electron transfer between MOF and CdS endows the hybrid outstanding photodegradation performance toward organic pollutants.

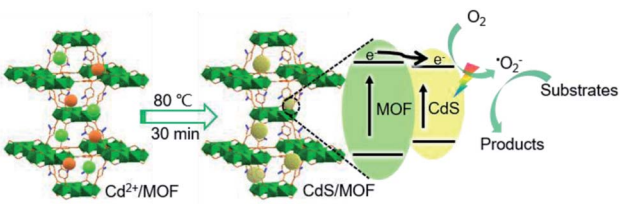

Scheme 1 Schematic illustration for the preparation of CdS/MOF hybrid.

Department of Chemistry, College of Chemistry and Chemical Engineering, Qingdao University, Qingdao, Shandong 266071, P. R. China. E-mail: chenzhen1738@163.com

† Electronic supplementary information (ESI) available. See DOI: 10.1039/d1ra05957b

© 2021 The Author(s). Published by the Royal Society of Chemistry

Open Access Article. Published on 02 November 2021. Downloaded on 1/10/2026 9:48:20 AM.
This article is licensed under a Creative Commons Attribution-NonCommercial 3.0 Unported Licence.

The crystallographic structure of CdS/NH_2-MIL-125 [7c,d] is analyzed and confirmed using powder X-ray diffraction (PXRD). As shown in Fig. 1a, the as-synthesized NH_2-MIL-125 has identical diffraction patterns as the simulated NH_2-MIL-125, which indicates the successful synthesis of MOF. For the diffraction patterns of CdS/NH_2-MIL-125, except for the typical diffraction peaks of MOF, two additional peaks appear at 2-theta values of 26.5° and 43.9° are assignable to CdS. And the peak intensities are enhanced along with increased CdS loadings. N_2 sorption experiments reveal that the Brunauer–Emmett–Teller (BET) surface areas of NH_2-MIL-125 and 15 wt% CdS/NH_2-MIL-125 are 956 and 613 $m^2\ g^{-1}$, respectively (Fig. 1b). The decreased surface areas indicate that CdS NPs may be successfully loaded on the MOF, and are well stabilized by the pores. The morphology of 15 wt% CdS/NH_2-MIL-125 is investigated by scanning electron microscopy (SEM). Fig. 1c shows the retained octahedral morphology of MOF with an average diameter of 200–300 nm. In addition, the transmission electron microscopy (TEM) image shows uniform dispersion of CdS particles (average size, 3.7 nm) throughout MOF (Fig. 1d), further demonstrating their successful assembly. The actual contents of CdS in CdS/NH_2-MIL-125 samples have been confirmed by inductively coupled plasma atomic emission spectrometry (ICP-AES). The percentages by weight of CdS are very close to the nominal values (Table S1, ESI†).

The cascade reaction between benzyl alcohol and malononitrile to produce benzylidene malononitrile under visible light irradiation has been investigated by CdS/NH_2-MIL-125. The reaction involves two steps including the first photocatalytic oxidation of benzyl alcohol to form benzaldehyde, and the second Knoevenagel reaction of benzaldehyde and malononitrile. As shown in Table 1, among different loadings of CdS in CdS/NH_2-MIL-125 samples, the catalytic performance of 15 wt% CdS/NH_2-MIL-125 is the best, which exhibits excellent conversion of 97% and good selectivity of 93% toward target product within 24 h (Table 1, entries 1–3). This may be due to easier aggregation of CdS particles with increased loadings and reduced active sites in low CdS contents. For comparison, their physical mixture shows lower activity (Table 1, entry 4), and NH_2-MIL-125 has no any photocatalytic activity (Table 1, entry 5), while CdS only catalyzes the first reaction to produce benzaldehyde with a conversion of 96% (Table 1, entry 6) under the same reaction conditions. In absence of visible light, no products are detected (Table 1, entry 7), and no reaction occurs without catalyst (Table 1, entry 8). In addition, reactions are also investigated in varying reaction conditions, such as different solvents, temperature, and reaction time (Table 1, entries 9–15). The optimal temperature is 80 °C, indicating the reaction temperature and time are crucial to the second step. In comparation, the reported catalysts for this one-pot cascade reaction display a lower yield or require higher temperature, high O_2 pressure and/or UV-light (Table S2, ESI†). These results highlight the important roles of each component in CdS/NH_2-MIL-125 and their excellent synergistic effects toward cascade reaction.

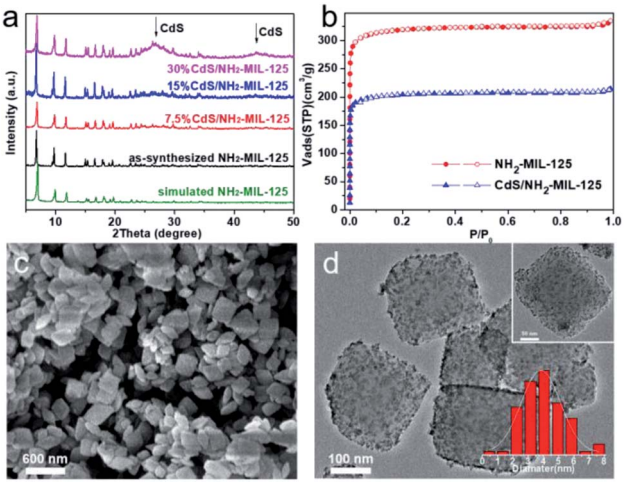

Fig. 1 (a) PXRD patterns of simulated NH_2-MIL-125, as-synthesized NH_2-MIL-125, and CdS/NH_2-MIL-125. (b) N_2 sorption isotherms of NH_2-MIL-125 and 15 wt% CdS/NH_2-MIL-125 at 77 K. (c) SEM and (d) TEM images of 15 wt% CdS/NH_2-MIL-125 and (inset in d) the corresponding size distribution of CdS NPs.

Inspired by the excellent catalytic performance of CdS/NH_2-MIL-125, another bifunctional CdS@MIL-101 catalyst based on the photocatalytic activity of CdS and Lewis acidity of MIL-101 is prepared (Fig. S1, ESI†). The retained crystallinity of MIL-101 upon loading CdS has been verified by PXRD patterns. The peak intensities of the CdS also increased with its higher loadings (Fig. S2, ESI†). The BET surface areas of as-synthesized MIL-101 and 15 wt% CdS@MIL-101 are 2900 and 2320 $m^2\ g^{-1}$, respectively, implying that MIL-101 cavities are possibly occupied by CdS NPs (Fig. S3, ESI†). The SEM image of CdS@MIL-101 shows the retained octahedral morphology of MIL-101 with an average diameter of 500–600 nm (Fig. S4, ESI†). The TEM image confirms uniform dispersion of CdS NPs (average size, 2.6 nm) throughout MOF, further demonstrating MOF cavities are successfully occupied by tiny CdS NPs (Fig. S5, ESI†). The cascade reaction involved photocatalytic oxidation of benzyl alcohol to benzaldehyde, and then aldimine condensation of benzaldehyde and aniline to give *N*-benzylideneaniline[1d,g] has been investigated by CdS@MIL-101. As expected, the hybrid material displays the best catalytic activity compared with those of CdS and MIL-101 alone (Table 2, entries 1 and 6). In order to investigate the influence of CdS levels on the reaction, CdS@MIL-101 samples with varying CdS content are synthesized. As the CdS loading increases, the color of composite gradually changed from green to yellow while the color from one batch keeps consistent. This reflects their successful assembly and uniform distribution of CdS NPs on MOF (Fig. S1, ESI†). The actual contents of CdS in CdS@MIL-101 are also analyzed by ICP-AES (Table S1, ESI†). Among these composites, the catalytic performance of 7.5 wt% CdS@MIL-101 is the best, which may be due to easier aggregation of CdS particles as increased loading and induced active sites in lower CdS contents (Table 2). In addition, the reactions are suppressed when DMF and methanol (MeOH) are applied as solvents or there is no light irradiation (Table 2, entries 7–9).

Organic pollutants such as dyes usually cause environmental pollution due to their degradation difficulties.[6b,12] However,

Open Access Article. Published on 02 November 2021. Downloaded on 1/10/2026 9:48:20 AM.
This article is licensed under a Creative Commons Attribution-NonCommercial 3.0 Unported Licence.

Table 1 Cascade reactions of benzyl alcohol oxidation followed by Knoevenagel condensation[a]

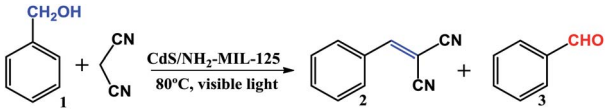

Entry	Catalyst	Time/h	Solvent	Conv. of 1	Select. of 2
1	15 wt% CdS/NH_2-MIL-125	24	CH_3CN	97%	93%
2	30 wt% CdS/NH_2-MIL-125	24	CH_3CN	86%	89%
3	7.5 wt% CdS/NH_2-MIL-125	24	CH_3CN	74%	91%
4[b]	CdS + NH_2-MIL-125	24	CH_3CN	20%	100%
5	NH_2-MIL-125	24	CH_3CN	—[c]	—
6	CdS	24	CH_3CN	96%	5%
7[d]	15 wt% CdS/NH_2-MIL-125	24	CH_3CN	—	—
8	No catalyst	24	CH_3CN	—	—
9	15 wt% CdS/NH_2-MIL-125	6	CH_3CN	69%	72%
10	15 wt% CdS/NH_2-MIL-125	16	CH_3CN	94%	80%
11	15 wt% CdS/NH_2-MIL-125	20	CH_3CN	96%	85%
12	15 wt% CdS/NH_2-MIL-125	24	DMF	—	—
13	15 wt% CdS/NH_2-MIL-125	24	MeOH	10%	100%
14[e]	15 wt% CdS/NH_2-MIL-125	24	CH_3CN	—	—
15[f]	15 wt% CdS/NH_2-MIL-125	24	CH_3CN	95%	73%
16	7.5 wt% CdS@MIL-101	24	CH_3CN	90%	—

[a] Reaction conditions: 0.5 mmol benzyl alcohol, 1.5 mmol malononitrile, 100 mg catalysts, 5 mL solvent, 80 °C, visible light ($\lambda \geq 420$ nm). [b] 15 mg CdS + 85 mg NH_2-MIL-125. [c] No products or negligible products. [d] Without visible light irradiation. [e] RT. [f] 50 °C.

Table 2 Cascade reaction of benzyl alcohol oxidation and the coupling reaction between benzaldehyde and aniline by different catalysts[a]

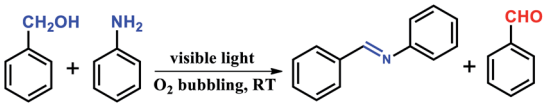

Entry	Catalyst	t (h)	Conv. (%)	Select. (%) –CHO	Select. (%) Product
1	CdS	2	30	100	
2	30 wt% CdS@MIL-101	2	62		100
		4	100		100
3	15 wt% CdS@MIL-101	2	56		100
		4	61		100
4	7.5 wt% CdS@MIL-101	2	90		100
		2.5	100		100
5	3.75 wt% CdS@MIL-101	2	41		100
6	MIL-101	2	0		
7[b]	7.5 wt% CdS@MIL-101	2	<10%		
8[c]	7.5 wt% CdS@MIL-101	2	<10%		
9[d]	7.5 wt% CdS@MIL-101	2	0		
10	15 wt% CdS/NH_2-MIL-125	2	<10%	100	

[a] Reaction conditions: 0.5 mmol benzyl alcohol, 0.5 mmol aniline, 10 mL toluene, visible light ($\lambda \geq 420$ nm), O_2 bubbling, 30 mg catalyst (CdS, 10 mg). [b] The solvent is DMF. [c] The solvent is MeOH. [d] Without light.

traditional treatment methods, such as membrane separation, adsorption, advanced oxidation, and microbial degradation are frequently tedious, costly and bring additional pollution and other problems.[13] Photocatalytic degradation of organic pollutants by solar energy has been deemed as an economical and environmentally friendly method.[14] Herein, degradation of organic dyes are investigated by CdS/NH_2-MIL-125 under visible light. UV-Vis spectrum is selected to evaluate the degradation efficiency (Fig. 2). As shown in Fig. 2a, ~90% of methyl violet (MV) decomposed after 20 min and almost completed after 60 min. As the degradation progresses, the color of the residual solution gradually become nearly colorless, demonstrating the successful degradation of MV (Fig. 2e). In comparation, a lower degradation rate of MV (only ~60%) by CdS is achieved (Fig. 2a). For safranine T, approximately 84% dye decomposed after 100 min using CdS/NH_2-MIL-125, while only 60% degradation is completed by CdS (Fig. 2b). Similarly, CdS/NH_2-MIL-125 exhibits a better degradation efficiency (80%) than that of CdS toward photocatalytic R250 degradation (47%) (Fig. 2c). Fig. 2d shows the gradually decreased absorption of methyl violet with prolonged illumination time. The similar phenomenon is also observed in other two dyes degradation (Fig. S4, ESI†). For three dyes, CdS/NH_2-MIL-125 exhibits superior photodegradation activity, primarily attributed to the following two factors: (1) the porosity of MOF improves the dispersion of small CdS particles, exposing more active sites; (2) effective electrons transfers from the photosensitive NH_2-MIL-125 to CdS and their synergistic effect significantly enhances the photocatalytic activity. In addition, CdS@MIL-101 with the same CdS loading has also been investigated for MV degradation and exhibits good

 © 2021 The Author(s). Published by the Royal Society of Chemistry

Open Access Article. Published on 02 November 2021. Downloaded on 1/10/2026 9:48:20 AM.
This article is licensed under a Creative Commons Attribution-NonCommercial 3.0 Unported Licence.

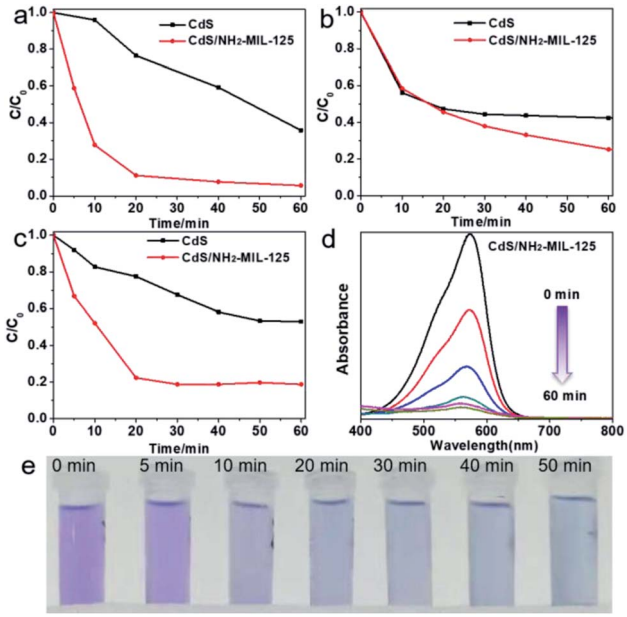

Fig. 2 Plots of photodegradation rate of (a) methyl violet, (b) safranine T and (c) coomassie brilliant blue R250 by catalysts (C_0 is the initial concentration and C is the concentration at any given time of the dye). (d) UV-Vis absorption spectra for methyl violet degradation by CdS/NH_2-MIL-125. (e) The changed solution color as the MV degradation proceeds using CdS/NH_2-MIL-125.

degradation rate (Fig. S6, ESI†), which is only slightly lower than that of 15 wt% CdS/NH_2-MIL-125.

According to UV-Vis diffuse reflectance spectra (DRS), CdS/NH_2-MIL-125 displays two absorption peaks in the region of 220–320 nm and 325–500 nm, combining both features of MOF and CdS (Fig. 3a). The absorption edge of CdS/NH_2-MIL-125 is red-shifted relative to NH_2-MIL-125, exhibiting better absorbance under visible light than pure MOF. The absorption edge of CdS@MIL-101 is also red-shifted relative to MIL-101 (Fig. S8, ESI†). In order to investigate the charge separation efficiency, the photocurrents of CdS/NH_2-MIL-125, NH_2-MIL-125 and CdS have been measured ($\lambda \geq 420$ nm). Among these samples, the strongest photocurrent density of CdS/NH_2-MIL-125 reflects that it has the most effective charge separation (Fig. 3b). The band gaps of NH_2-MIL-125, CdS and CdS/NH_2-MIL-125 composite have been calculated based on Tauc plots (Fig. 3c). The band gap of CdS/NH_2-MIL-125 (2.18 eV) is very close to that of CdS (2.1 eV), and obviously below that of NH_2-MIL-125 (2.46 eV). The introduced CdS narrows the band gap of NH_2-MIL-125. This indicates that CdS/NH_2-MIL-125 is more effective on visible-light utilization compared with NH_2-MIL-125. Fig. 3d shows the Mott–Schottky plot of CdS and NH_2-MIL-125 in a 0.5 M Na_2SO_4 aqueous solution. All plots have a positive slope, which reveals the typical n-type semiconductor characteristics for NH_2-MIL-125 and CdS. The flat band potential (E_{fb}) of NH_2-MIL-125 and CdS are −0.91 eV (*vs.* Ag/AgCl) or −1.34 eV (absolute value), and −0.86 eV (*vs.* Ag/AgCl) or −1.29 eV (absolute value), respectively. They are close to the conduction bands in reported n-type semiconductors.[15]

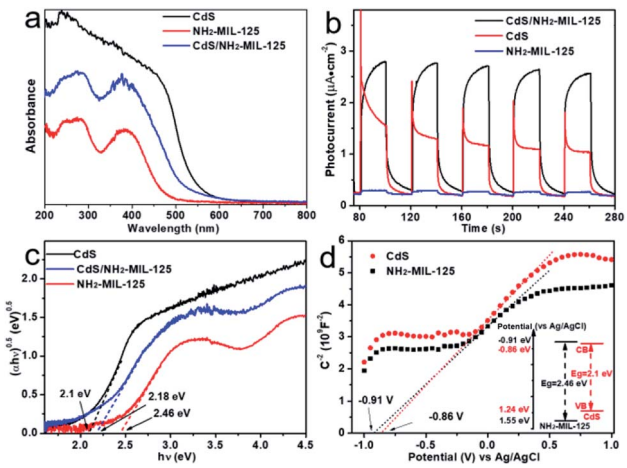

Fig. 3 (a) UV-Vis DRS and (b) photocurrent test of samples. (c) Tauc plots of samples. (d) Mott–Schottky plots of CdS and NH_2-MIL-125 in a 0.5 M Na_2SO_4 aqueous solution.

By combining photo-degradation with DRS data, we propose a possible mechanism to illustrate the synergistic effects between CdS and NH_2-MIL-125 (Fig. S9, ESI†). The possible electron transfer from NH_2-MIL-125 to CdS is contribute to the production of reactive oxygen species and further enhances dyes photodegradation activity.[7] In addition, the porous structure of MOF effectively improves the highly dispersed CdS NPs, and facilitates substrates transport (Fig. S10, ESI†).

In summary, a bifunctional CdS/NH_2-MIL-125 with excellent photocatalytic performance has been synthesized. Its superior catalytic activity toward a one-pot cascade reaction is mainly attributed to the cooperative effect that CdS provides photocatalysis activity, while NH_2-MIL-125 acts as a porous carrier to disperse CdS NPs effectively and provides Lewis base sites. Simultaneously, another bifunctional CdS@MIL-101 catalyst displays comparable activity toward another cascade reaction based on photooxidation activity of CdS and Lewis acidity of MIL-101. Furthermore, effective electron transfer from excited NH_2-MIL-125 to CdS helps slow down the charge-recombination process in CdS and enhances the synergetic photodegradation activity. It is expected that this work could provide new insight into the design and preparation of MOF-based multifunctional photocatalysts.

Conflicts of interest

There are no conflicts to declare.

Acknowledgements

The authors are grateful to financial support by Excellent Youth Foundation of Shandong Province (ZR2020YQ08) and Key Research and Development Program of Shandong Province (2019GGX103043).

Notes and references

1 (*a*) V. P. Mehta and E. V. V. Eycken, *Chem. Soc. Rev.*, 2011, **40**, 4925–4936; (*b*) L. F. Tietze, *Chem. Rev.*, 1996, **96**, 115–136; (*c*)

Open Access Article. Published on 02 November 2021. Downloaded on 1/10/2026 9:48:20 AM.
This article is licensed under a Creative Commons Attribution-NonCommercial 3.0 Unported Licence.

B. List, *Angew. Chem., Int. Ed.*, 2010, **49**, 1730–1734; (*d*) B. Gnanaprakasam, J. Zhang and D. Milstein, *Angew. Chem., Int. Ed.*, 2010, **49**, 1468–1471; (*e*) R. K. Shiroodi and V. Gevorgyan, *Chem. Soc. Rev.*, 2013, **42**, 4991–5001; (*f*) X. Li, B. Lin, H. Li, Q. Yu, Y. Ge, X. Jin, X. Liu, Y. Zhou and J. Xiao, *Appl. Catal., B*, 2018, **239**, 254–259; (*g*) R. Wu, S. Wang, Y. Zhou, J. Long, F. Dong and W. Zhang, *ACS Appl. Nano Mater.*, 2019, **2**, 6818–6827.

2 (*a*) J.-J. Zhu, K. Kailasam, A. Fischer and A. Thomas, *ACS Catal.*, 2011, **1**, 342–347; (*b*) P.-P. Wu, Y. X. Cao, L. M. Zhao, Y. Wang, Z. K. He, W. Xing, P. Bai, S. Mintova and Z. F. Yan, *J. Catal.*, 2019, **375**, 32–43; (*c*) U. P. N. Tran, K. K. A. Le and N. T. S. Phan, *ACS Catal.*, 2011, **1**, 120–127; (*d*) A. Rashidizadeh, H. R. E. Zand, H. Ghafuri and Z. Rezazadeh, *ACS Appl. Nano Mater.*, 2020, **3**, 7057–7065.

3 (*a*) Q. Xu, B. Cheng, J. Yu and G. Liu, *Carbon*, 2017, **118**, 241–249; (*b*) Y.-P. Wu, B. Yang, J. Tian, S.-B. Yu, H. Wang, D.-W. Zhang, Y. Liu and Z.-T. Li, *Chem. Commun.*, 2017, **53**, 13367–13370; (*c*) Y. Li, M. Liu and L. Chen, *J. Mater. Chem. A*, 2017, **5**, 13757–13762; (*d*) S. Meng, X. Ning, S. Chang, X. Fu, X. Ye and S. Chen, *J. Catal.*, 2018, **357**, 247–256; (*e*) Y. Zhang, J. Zhou, J. Chen, X. Feng and W. Cai, *J. Hazard. Mater.*, 2020, **392**, 122315.

4 L. Cheng, Q. Xiang, Y. Liao and H. Zhang, *Energy Environ. Sci.*, 2018, **11**, 1362–1391.

5 (*a*) M. A. Nasalevich, M. van der Veen, F. Kapteijn and J. Gascon, *CrystEngComm*, 2014, **16**, 4919; (*b*) J. L. Gong, C. Li and M. R. Wasielewski, *Chem. Soc. Rev.*, 2019, **48**, 1862–1864.

6 (*a*) J. Li, J. Yang, F. Wen and C. Li, *Chem. Commun.*, 2011, **47**, 7080–7082; (*b*) X. Li, J. Zhu and H. Li, *Appl. Catal., B*, 2012, **123–124**, 174–181; (*c*) N. Zhang, M.-Q. Yang, Z.-R. Tang and Y.-J. Xu, *J. Catal.*, 2013, **303**, 60–69; (*d*) W. Chen, J. Fang, Y. Zhang, G. Chen, S. Zhao, C. Zhang, R. Xu, J. Bao, Y. Zhou and X. Xiang, *Nanoscale*, 2018, **10**, 4463–4474.

7 (*a*) L. Shen, S. Liang, W. Wu, R. Liang and L. Wu, *J. Mater. Chem. A*, 2013, **1**, 11473–11482; (*b*) Z. Jiang, J. Liu, M. Gao, X. Fan, L. Zhang and J. Zhang, *Adv. Mater.*, 2017, **29**, 1603369; (*c*) H.-Q. Xu, S. Yang, X. Ma, J. H. Huang and H.-L. Jiang, *ACS Catal.*, 2018, **8**, 11615–11621; (*d*) S. Gao, W. Cen, Q. Lia, J. Li, Y. Lu, H. Wang and Z. Wu, *Appl. Catal., B*, 2018, **227**, 190–197.

8 (*a*) H. Deng, S. Grunder, K. E. Cordova, C. Valente, H. Furukawa, M. Hmadeh, F. Gándara, A. C. Whalley, Z. Liu and S. Asahina, *Science*, 2012, **336**, 1018–1023; (*b*) H.-C. Zhou and S. Kitagawa, *Chem. Soc. Rev.*, 2014, **43**, 5415–5418; (*c*) B. Liang, X. Zhang, Y. Xie, R.-B. Lin, R. Krishna, H. Cui, Z. Li, Y. Shi, H. Wu, W. Zhou and B. Chen, *J. Am. Chem. Soc.*, 2020, **142**, 17795; (*d*) L. Chen and Q. Xu, *Matter*, 2019, **1**, 57–89; (*e*) L. Wang, S.-R. Li, Y.-Z. Chen and H.-L. Jiang, *Small*, 2021, **17**, 2004481.

9 (*a*) A. Dhakshinamoorthy and H. Garcia, *Chem. Soc. Rev.*, 2012, **41**, 5262; (*b*) K. M. Choi, K. Na, G. A. Somorjai and O. M. Yaghi, *J. Am. Chem. Soc.*, 2015, **137**, 7810–7816; (*c*) H. Liu, L. Chang, C. Bai, L. Chen, R. Luque and Y. Li, *Angew. Chem., Int. Ed.*, 2016, **55**, 5019–5023; (*d*) A. Dhakshinamoorthy, M. Alvaro and H. Garcia, *Chem. Commun.*, 2012, **48**, 11275–11288; (*e*) Y.-Z. Chen, R. Zhang, L. Jiao and H.-L. Jiang, *Coord. Chem. Rev.*, 2018, **362**, 1–23; (*f*) J.-D. Xiao and H.-L. Jiang, *Acc. Chem. Res.*, 2019, **52**, 356–366; (*g*) C. N. Neumann, S. J. Rozeveld, M. Yu, A. J. Rieth and M. Dincă, *J. Am. Chem. Soc.*, 2019, **141**, 17477; (*h*) M. Fiaz, M. Kashif, M. Fatima, S. R. Batool, M. A. Asghar, M. Shakeel and M. Athar, *Catal. Lett.*, 2020, **150**, 2648–2659; (*i*) K. Sun, M. Liu, J. Pei, D. Li, C. Ding, K. Wu and H.-L. Jiang, *Angew. Chem., Int. Ed.*, 2020, **59**, 22749–22755; (*j*) S. Dai, A. Tissot and C. Serre, *Adv. Energy Mater.*, 2021, 2100061.

10 (*a*) T. Zhang and W. Lin, *Chem. Soc. Rev.*, 2014, **43**, 5982–5993; (*b*) G. Zhang, M. Zhang, X. Qiu and X. Wang, *Adv. Mater.*, 2014, **26**, 805–809; (*c*) D. Wang, M. Wang and Z. Li, *ACS Catal.*, 2015, **5**, 6852–6857; (*d*) H. Zhang, G. Liu, L. Shi, H. Liu, T. Wang and J. Ye, *Nano Energy*, 2016, **22**, 149–168; (*e*) A. Dhakshinamoorthy, A. M. Asiri and H. García, *Angew. Chem., Int. Ed.*, 2016, **55**, 5414–5445; (*f*) D. Shi, R. Zheng, M. J. Sun, X. Cao, C. X. Sun, C. J. Cui, C. S. Liu, J. Zhao and M. Du, *Angew. Chem.*, 2017, **56**, 14637–14641; (*g*) Y. Xiao, Y. Qi, X. Wang, X. Wang, F. Zhang and C. Li, *Adv. Mater.*, 2018, **30**, 1803401; (*h*) L. Chen, F. Yu, X. Shen and C. Duan, *Chem. Commun.*, 2019, **55**, 4845–4848; (*i*) X. Li and Q.-L. Zhu, *EnergyChem*, 2020, **2**, 100033; (*j*) Y. Xue, G. Zhao, R. Yang, F. Chu, J. Chen, L. Wang and X. Huang, *Nanoscale*, 2021, **13**, 3911–3936; (*k*) Y. Pan, Y. Qian, X. Zheng, S.-Q. Chu, Y. Yang, C. Ding, X. Wang, S.-H. Yu and H.-L. Jiang, *Natl. Sci. Rev.*, 2021, **8**, nwaa224.

11 (*a*) S. Yang, B. Pattengale, E. L. Kovrigin and J. Huang, *ACS Energy Lett.*, 2017, **2**, 75–80; (*b*) J.-D. Xiao, L. Han, J. Luo, S.-H. Yu and H.-L. Jiang, *Angew. Chem., Int. Ed.*, 2018, **57**, 1103–1107.

12 J.-J. Du, Y.-P. Yuan, J.-X. Sun, F.-M. Peng, X. Jiang, L.-G. Qiu, A.-J. Xie, Y.-H. Shen and J.-F. Zhu, *J. Hazard. Mater.*, 2011, **190**, 945–951.

13 (*a*) K. He, G. Q. Chen, G. M. Zeng, A. W. Chen, Z. Z. Huang, J. B. Shi, T. T. Huang, M. Peng and L. Hua, *Appl. Catal., B*, 2018, **228**, 19–28; (*b*) X. Zhao, X. J. Zhang, D. X. Han and L. Niu, *Appl. Surf. Sci.*, 2020, **501**, 144258; (*c*) Q. Zhao, H. Y. Xiao, G. Huangfu, Z. P. Zheng, J. S. Wang, F. F. Wang and Y. P. Guo, *Nano Energy*, 2021, **85**, 106028.

14 (*a*) H. Chen, K. Shen, J. Chen, X. Chen and Y. Li, *J. Mater. Chem. A*, 2017, **5**, 9937; (*b*) N. Liu, W. Huang, X. Zhang, L. Tang, L. Wang, Y. Wang and M. Wu, *Appl. Catal., B*, 2018, **221**, 119; (*c*) S. He, Q. Rong, H. Niu and Y. Cai, *Appl. Catal., B*, 2019, **247**, 49; (*d*) X. M. Liu, X. Y. Chen, Y. Z. Li, B. Q. Wu, X. B. Luo, S. Ouyang, S. L. Luo, A. A. Al Kheraifd and J. Lin, *J. Mater. Chem. A*, 2019, **7**, 19173–19186; (*e*) Y. Wang, H. Wang, J. Lia and X. Zhao, *Appl. Catal., B*, 2020, **278**, 118981.

15 W. Hou, M. Chen, C. Chen, Y. Wang and Y. Xu, *J. Colloid Interface Sci.*, 2021, **604**, 310–318.

 © 2021 The Author(s). Published by the Royal Society of Chemistry